AGU ADVANCING EARTH AND SPACE SCIENCE

Geophysical Research Letters®

RESEARCH LETTER
10.1029/2021GL094292

Key Points:

- Influence of matrix diffusion on concentration power spectra and catchment solute travel time distributions is quantified theoretically
- Matrix diffusion produces fractal scaling in stream concentration power spectra when combined with variable advective travel times
- 1/frequency spectral filtering identified in stream chloride power spectrum at Lower Hafren is reproduced by matrix diffusion model

Supporting Information:

Supporting Information may be found in the online version of this article.

Correspondence to:

H. Rajaram,
hrajara1@jhu.edu

Citation:

Rajaram, H. (2021). Matrix diffusion as a mechanism contributing to fractal stream chemistry and long-tailed transit time distributions. *Geophysical Research Letters*, *48*, e2021GL094292. https://doi.org/10.1029/2021GL094292

Received 24 MAY 2021
Accepted 1 SEP 2021

Matrix Diffusion as a Mechanism Contributing to Fractal Stream Chemistry and Long-Tailed Transit Time Distributions

Harihar Rajaram[1]

[1]Department of Environmental Health and Engineering, Johns Hopkins University, Baltimore, MD, USA

Abstract Solute transit or travel time distributions (TTDs) in catchments are relevant to both hydrochemical response and inference of hydrologic mechanisms. Long-tailed TTDs and fractal scaling behavior of stream concentration power spectra (~1/frequency, or 1/frequency to a power <2) are widely observed in catchment studies. In several catchments, a significant fraction of streamflow is derived from groundwater in shallow fractured bedrock, where matrix diffusion significantly influences solute transport. I present frequency and time domain theoretical analyses of solute transport to quantify the influence of matrix diffusion on fractal scaling and long-tailed TTDs. The theoretical concentration power spectra exhibit fractal scaling, and the corresponding TTDs resemble a gamma distribution. The tails of the TTDs are influenced by accessible matrix width, exhibiting a sustained power-law (rather than exponential) decline for large matrix widths. Application to an experimental catchment shows that theoretical spectra match previously reported power spectral estimates derived from concentration measurements.

Plain Language Summary A significant fraction of rainfall on catchments flows as groundwater before discharging to a river. Groundwater in catchments is often hosted in shallow fractured bedrock. In these systems, solutes dissolved in rainfall are transported relatively rapidly by water flowing in rock fractures. However, some of the solutes diffuse from fractures into the tiny pores of the rock matrix where water is not flowing. This phenomenon is referred to as matrix diffusion and leads to retention and slow long-term release of solutes. It regulates the flushing rate of contaminants (e.g., agricultural chemicals) and chemicals input by atmospheric deposition from catchments, and must be considered when inferring internal catchment processes based on solute measurements. This paper develops theoretical equations to describe the transport and retention of solutes in catchments underlain by fractured bedrock, and the delivery of solutes to rivers. These theoretical equations explain interesting features of observed solute concentration variations in rivers and can be used to model catchment response to contamination.

1. Introduction

The transport and retention of solutes in catchments is influenced by both hydrologic and biogeochemical processes. Solute transit or travel time distributions (TTDs) provide insights on the integrated behavior of hydrologic and biogeochemical processes within catchments, although the distinction between the processes and time scales involved in hydrologic/hydraulic versus hydrochemical response should be emphasized (Birkel et al., 2011; Botter et al., 2010; Fiori & Russo, 2008; Hrachowitz et al., 2013; Maloszewski & Zuber, 1993; McGuire & McDonnell, 2006). There is a large body of research on TTDs in catchments, which has been synthesized in review papers (e.g., Hrachowitz et al., 2016; Maloszewski & Zuber, 1993; McGuire & McDonnell, 2006; Sprenger et al., 2019).

Catchment solute TTDs often exhibit longer tails than the exponential distribution, a commonly used model for TTDs. Additionally, Kirchner et al. (2000, 2001) showed that solute TTDs in catchments at Plynlimon, UK, decline more steeply than an exponential distribution at early times. They suggested that a gamma distribution, $h(t) = \left(t^{\alpha-1}e^{-t/\beta}\right)/\left(\beta^{\alpha}\Gamma(\alpha)\right)$, with shape parameter $\alpha = 0.5$ (more generally $\alpha < 1$), captures both steep early-time decline (indicative of short-term responsiveness) and long-term memory and is hence a better model for solute TTDs than the exponential distribution ($\alpha = 1$). Correspondingly, stream concentration

power spectra were observed to exhibit 1/frequency behavior (more generally 1/frequency to a power <2) across a wide range of frequencies, which they referred to as "fractal stream chemistry." Similar behavior has been documented at other catchments (Godsey et al., 2010), and for a variety of solutes (Kirchner & Neal, 2013), although some catchments do exhibit exponential baseflow TTDs (e.g., McGuire et al., 2005).

Various mechanisms have been proposed to explain fractal stream chemistry. Kirchner et al. (2001); Kirchner and Neal (2013) suggested that this behavior could result from an advective-dispersive process with high dispersion (Peclet number [Pe] ~1), associated with variable travel time across streamlines in a hillslope flow system. Lindgren et al. (2004) proposed that even with moderate dispersion, first-order mobile-immobile exchange can explain fractal scaling. Cardenas (2007) and Kollet and Maxwell (2008) demonstrated that hillslope groundwater flow systems with significant variation in advective travel times across streamlines produce power-law solute TTDs. Kollet and Maxwell (2008) also showed that transient vadose zone processes influence stream concentration spectra at higher frequencies. Fiori and Russo's (2008) simulations of transient flow and solute transport in a hillslope produced TTDs resembling gamma distributions with $\alpha < 1$. Haitjema (1995) and Fiori and Russo (2008) showed that transient effects and heterogeneity have a minor influence on TTDs compared to variations in travel times across streamlines in steady flow representations. Ameli et al. (2016) showed that decreasing permeability with depth in a hillslope flow model, either exponential or due to macroscopic layering, produced a gamma TTD with α close to 0.5. Harman (2015) showed that a time-variable uniform TTD with a range parameter that increases with decreasing storage (inverse storage effect) reproduces 1/frequency spectra. Lumped parameter hydrochemical models with multiple compartments have also reproduced gamma TTDs with $\alpha < 1$ (Benettin et al., 2015; Hrachowitz et al., 2013).

The contribution of shallow groundwater flow through fractured bedrock to streamflow and solute export in mountain catchments has long been recognized, including at Plynlimon (Kirchner et al., 2001; Neal et al., 1997) and other recent studies (Carroll et al., 2019, 2020; Frisbee et al., 2013; Godsey et al., 2010; Hale et al., 2016; Herndon et al., 2015; Manning et al., 2013; Tokunaga et al., 2019). It is well established that matrix diffusion, a phenomenon first invoked to explain anomalous tracer ages (Foster, 1975; Neretnieks, 1981), significantly influences the travel time of tracers in fractured rock. The potential influence of matrix diffusion on catchment hydrochemical response and tracer ages was further highlighted by Maloszewski and Zuber (1993) and Shapiro (2011). However, few models of catchment-scale solute TTDs explicitly incorporate the influence of matrix diffusion, and its contribution to fractal scaling and long-tailed TTDs has not received sufficient attention. In this paper, I present frequency and time domain analyses of the combined influence of variable advective travel times and matrix diffusion on solute transport in a catchment/hillslope groundwater system hosted in fractured bedrock. I show that the theoretical power spectrum of stream concentration variations inherently exhibits fractal scaling, and that the solute TTD strongly resembles a gamma distribution with $\alpha < 1$ for finite accessible matrix widths. For larger matrix widths, the characteristic late-time power-law tailing associated with matrix diffusion persists for a long duration. I also present an application to the Lower Hafren catchment at Plynlimon.

2. Conceptual Model and Transport Equations

The catchment-scale groundwater flow system is represented as a steady saturated flow in fractured bedrock, receiving spatially uniform recharge. Figure 1 shows a schematic representation (adapted from Haitjema, 1995). Fluid flow is assumed to occur only in fractures, with no advection in the rock matrix. Solutes undergo rapid advection along streamlines through permeable fractures, while simultaneously diffusing in and out of the rock matrix. The fracture density is assumed to be high so that an equivalent porous medium representation is employed for flow (but not for transport). Thus, the water table and hydraulic head field are assumed to be well defined and smooth. Isochrones I_{T_a} denote contours of equal advective travel time T_a from the water table to the outflow at the stream, and Ω_{T_a} denotes the surface area contained within I_{T_a}. Advective travel times T_a along streamlines (streamsurfaces) from the water table to the stream are assumed to increase monotonically with Ω_{T_a}. The streamtube originating from the surface element $d\Omega_{T_a}$ in Figure 1a is bounded by isochrones I_{T_a} and $I_{T_a+dT_a}$, comprising streamlines along which advective travel times to the stream range from T_a to $T_a + dT_a$. It is important to emphasize the distinction between advective and total solute travel times: the total travel time along a streamline is also influenced by matrix diffusion and thus

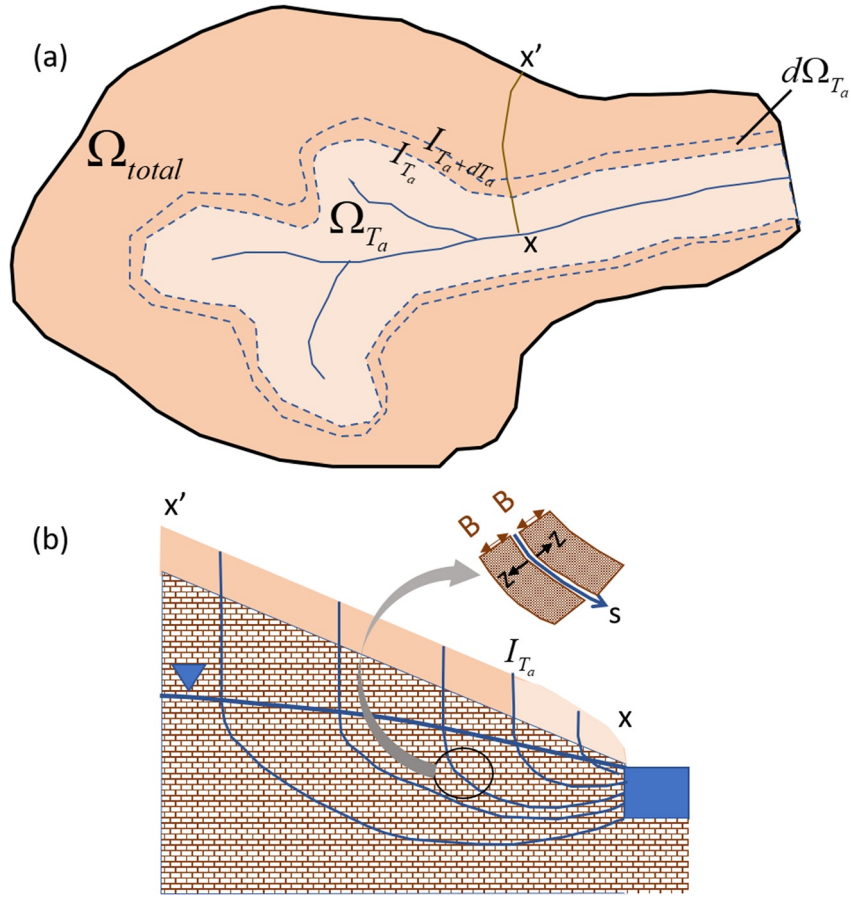

Figure 1. Schematic conceptual model of catchment-scale groundwater flow and transport. (a) Plan view showing total area Ω_{total} and area Ω_{T_a} bounded by isochrone I_{T_a} from which the advective travel time to the stream is T_a. (b) Vertical cross-section along x-x′ in (a), showing streamlines from the surface, through the water table to the stream. The streamline coordinate is denoted by s, and z denotes the distance from the fracture-matrix interface. One-dimensional matrix diffusion is assumed, with an accessible matrix width B.

much longer than the advective travel time. The catchment-scale solute TTD is derived by considering the distribution of total travel/transit times across all streamlines.

Previous studies suggest that when advective travel times across streamlines vary over a large range, the influence of heterogeneity and dispersion is secondary (Duffy & Gelhar, 1986; Fiori & Russo, 2008; Gelhar, 1993; Haitjema, 1995). I therefore neglect streamline tortuosity and dispersion in the analysis presented below. The influence of heterogeneity may be incorporated using modified advective travel time distributions as in the Lagrangian stochastic frameworks of Cvetkovic et al. (1999) and Simic and Destouni (1999). I assume one-dimensional diffusion with an effective matrix width B (Figure 1b), which may either be related to the block size or an accessible weathered matrix thickness adjacent to fractures. Multidimensional diffusion in matrix blocks is similar to one-dimensional diffusion with modified parameters, as discussed by Barker (1985).

For the above flow system, solute transport equations along a streamline and the matrix domain adjacent to it are presented below, following Grisak and Pickens (1980), Tang et al. (1981), and Małoszewski and Zuber (1985). The fracture concentration at time t, at location s along a streamline that originated at isochrone I_{T_a} (Figure 1) is denoted by $C_f\left(s,t;I_{T_a}\right)$; and the concentration in the adjacent rock matrix by $C_m\left(s,z,t;I_{T_a}\right)$, where z is the distance from the fracture matrix interface (see Figure 1b). The fracture transport equation is:

$$\frac{\partial C_f}{\partial t} + u_s \frac{\partial C_f}{\partial s} = \frac{2\phi_m D_e}{b}\left(\frac{\partial C_m}{\partial z}\right)_{s,z=0,t} \tag{1}$$

where u_s is the solute velocity along the streamline, b is the fracture aperture; ϕ_m and D_e are the matrix porosity and effective diffusivity respectively. The parameters b, ϕ_m, and D_e are assumed as constant catchment-scale average values, while u_s varies across the flow system. The diffusion equation in the rock matrix is:

$$\left(\phi_m + \rho_b K_d\right)\frac{\partial C_m}{\partial t} - \phi_m D_e \frac{\partial^2 C_m}{\partial z^2} = 0 \tag{2}$$

where ρ_b and $K_d$are respectively the bulk density of solids and the distribution coefficient in the rock matrix. The lateral boundary conditions for Equation 2 are:

$$C_m\left(s, z = 0, t; I_{T_a}\right) = C_f\left(s, t; I_{T_a}\right), \quad \frac{\partial C_m}{\partial z}\left(s, z = B, t; I_{T_a}\right) = 0 \tag{3}$$

The streamline coordinate s in Equation 1 may be replaced with an advective travel time coordinate (Cvetkovic et al., 1999; Duffy & Gelhar, 1986; Gelhar & Collins, 1971):

$$\tau_a = \int_{s'=0}^{s} \frac{ds'}{u_s\left(s'\right)} \tag{4}$$

Correspondingly, the fracture and matrix concentrations may be written as functions of τ_a, that is, $C_f\left(\tau_a, t; I_{T_a}\right)$ and $C_m\left(\tau_a, z, t; I_{T_a}\right)$, and Equation 1 can be rewritten as (Cvetkovic et al., 1999):

$$\frac{\partial C_f}{\partial t} + \frac{\partial C_f}{\partial \tau_a} = \frac{2\phi_m D_e}{b}\left(\frac{\partial C_m}{\partial z}\right)_{\tau_a, z=0, t} \tag{5}$$

I use Equation 5, together with Equations 2 and 3 to relate the stream concentration to the input concentration. At the inflow end of a streamline ($s = 0$, $\tau_a = 0$), concentration inputs $C_i\left(t\right)$ are assumed to be uniform across all streamlines (i.e., the catchment area), but vary with time:

$$C_f\left(\tau_a = 0, t; I_{T_a}\right) = C_i\left(t\right) \tag{6}$$

At the outflow boundary $\left(\tau_a = T_a\right)$, the stream concentration $C_o\left(t\right)$ is obtained by mixing of concentrations from all streamlines. The fraction of the total outflow that originates within the streamtube $d\Omega_{T_a}$ is denoted as $w\left(I_{T_a}\right)d\Omega_{T_a}$, where $w\left(I_{T_a}\right)$ is a flux-weighting function. If T_a increases monotonically with Ω_{T_a}, the fraction $w\left(I_{T_a}\right)d\Omega_{T_a}$ may also be represented using the advective travel time probability density function across streamlines, $P\left(T_a\right)$, as $P\left(T_a\right)dT_a$. Thus, $C_o\left(t\right)$ may be written in terms of an integral over either Ω_{T_a} or T_a:

$$C_o\left(t\right) = \int_{\Omega_{\text{total}}} C_f\left(T_a, t; I_{T_a}\right) w\left(I_{T_a}\right) d\Omega_{T_a} = \int_{T_a=0}^{\infty} C_f\left(T_a, t; I_{T_a}\right) P\left(T_a\right) dT_a \tag{7}$$

If the fluid flux and velocity are assumed to be constant across the depth of the flow system at the outflow, as in a Dupuit model, $w\left(I_{T_a}\right) = 1/\Omega_{\text{total}}$, a constant. Additionally, assuming spatially uniform recharge and an approximately constant saturated thickness (H), $P\left(T_a\right)$ is an exponential distribution (Gelhar & Wilson, 1974; Haitjema, 1995; Małoszewski & Zuber, 1982):

$$P\left(T_a\right) = \frac{1}{\bar{T}_a}\exp\left(-\frac{T_a}{\bar{T}_a}\right) \tag{8}$$

In Equation 8, $\bar{T}_a$ is the mean advective travel time, given by $\phi_a H / r$, where ϕ_a is the active porosity corresponding to the hydrologically responsive fracture flow system and r is the recharge rate. The exponential advective travel time distribution is also applicable to hillslope flow systems with a sloping base, under the assumption of uniform recharge and constant saturated thickness. The relationship for Ω_{T_a} corresponding to Equation 8 is (Haitjema, 1995):

$$\Omega_{T_a} = \Omega_{\text{total}}\left(1 - \exp\left(-T_a/\bar{T}_a\right)\right) \tag{9}$$

3. Frequency Domain Analysis: Stream Concentration Power Spectrum

To relate the power spectra of stream and precipitation concentrations, the transport equations are solved in the frequency domain (Sections S.1 and S.2). The Fourier transforms (or spectral representations) of $C_i\left(t\right), C_o\left(t\right), C_f\left(\tau_a, t; I_{T_a}\right)$ and $C_m\left(\tau_a, z, t; I_{T_a}\right)$ are denoted by $\tilde{C}_i\left(\omega\right), \tilde{C}_o\left(\omega\right), \tilde{C}_f\left(\tau_a, \omega; I_{T_a}\right)$ and $\tilde{C}_m\left(\tau_a, z, \omega; I_{T_a}\right)$ respectively, where ω is the angular frequency. The Fourier transforms of Equations 2 and 3 are solved to

express $\tilde{C}_m\left(\tau_a, z, \omega; I_{T_a}\right)$ in terms of $\tilde{C}_f\left(\tau_a, \omega; I_{T_a}\right)$ (Equation S7). Using this relationship in the Fourier transform of Equation 5 produces a differential Equation S8 for $\tilde{C}_f\left(\tau_a, \omega; I_{T_a}\right)$:

$$\frac{d\tilde{C}_f}{d\tau_a} + k(\omega)\tilde{C}_f = 0 \tag{10}$$

where (Equations S10 and S11):

$$k(\omega) = i\omega + \frac{2\phi_m\sqrt{RD_e\omega}}{b}\sqrt{i} - \frac{\frac{4\phi_m\sqrt{RD_e\omega}}{b}\sqrt{i}}{\left(1+\exp\left(2\sqrt{\frac{R\omega}{D_e}}B\sqrt{i}\right)\right)} \tag{11}$$

In Equation 11, $i = \sqrt{-1}$ and $R = \left(1 + \rho_b K_d/\phi_m\right)$ denotes the retardation factor in the rock matrix.

Solving Equation 10 and using the transform of Equation 6, the Fourier transform of the fracture concentration at the outflow end of a streamline ($\tau_a = T_a$) is:

$$\tilde{C}_f\left(T_a, \omega; I_{T_a}\right) = \tilde{C}_i(\omega)\exp\left\{-k(\omega)T_a\right\} \tag{12}$$

The Fourier transform of the stream concentration is then obtained from Equation 7:

$$\tilde{C}_o(\omega) = \tilde{C}_i(\omega)\int_0^\infty \exp\left\{-k(\omega)T_a\right\}P(T_a)dT_a \tag{13}$$

Correspondingly, the stream $\left(S_{C_oC_o}(\omega)\right)$ and precipitation $\left(S_{C_iC_i}(\omega)\right)$ concentration power spectra are related by:

$$S_{C_oC_o}(\omega) = S_{C_iC_i}(\omega)\left|\int_0^\infty \exp\left\{-k(\omega)T_a\right\}P(T_a)dT_a\right|^2 \tag{14}$$

Equation 14 generalizes a relationship presented by Duffy and Gelhar (1985) and Gelhar (1993) for pure advection ($k(\omega) = i\omega$), by incorporating matrix diffusion and reformulating the integral in terms of $P(T_a)$. In general, any appropriate advective travel time distribution (obtained from an analytical or numerical groundwater flow model) can be employed in Equation 14.

For the exponential advective travel time distribution, the stream concentration power spectrum is obtained by using Equations 11 and 8 in Equation 14 (Section S.2):

$$S_{C_oC_o}(\omega) = S_{C_iC_i}(\omega)\frac{1}{1 + 2\sqrt{2}AM\sqrt{\omega\overline{T_a}} + 2A^2\left(M^2+N^2\right)\omega\overline{T_a} + 2\sqrt{2}AN\left(\omega\overline{T_a}\right)^{3/2} + \omega^2\overline{T_a}^2} \tag{15}$$

where

$$A = \frac{\phi_m\sqrt{RD_e\overline{T_a}}}{b}, m = 1 + \exp\left(\sqrt{2\omega\overline{T_a}}\frac{B\sqrt{R}}{\sqrt{D_e\overline{T_a}}}\right)\cos\left(\sqrt{2R\omega\overline{T_a}}\frac{B\sqrt{R}}{\sqrt{D_e\overline{T_a}}}\right)$$
$$n = \exp\left(\sqrt{2\omega\overline{T_a}}\frac{B\sqrt{R}}{\sqrt{D_e\overline{T_a}}}\right)\sin\left(\sqrt{2\omega\overline{T_a}}\frac{B\sqrt{R}}{\sqrt{D_e\overline{T_a}}}\right), M = 1 - \frac{2(m+n)}{m^2+n^2}, N = 1 - \frac{2(m-n)}{m^2+n^2} \tag{16}$$

Equation 15 is written in terms of a dimensionless frequency ($\omega\overline{T_a}$) to highlight the dimensionless parameters that regulate the influence of matrix diffusion. The dimensionless parameter A is a measure of the strength of matrix diffusion. It may also be viewed as a ratio between the matrix storage accessible over a time scale on the order of $\overline{T_a}$ (which scales with the retardation factor times the retarded diffusion thickness, that is, $\sqrt{RD_e\overline{T_a}}$) and the fracture storage (which scales with b). For illustration, with representative values of $\phi_m = 0.05, D_e = 10^{-10}$ m^2/s, $b = 10^{-4}$ m, and $R = 1$; $\overline{T_a} = 2$ and 10 days will respectively yield $A = 2.08$ and 4.65. The parameter $B/\sqrt{D_e\overline{T_a}/R}$ represents the influence of matrix thickness. If $B >>$ the accessible matrix diffusion thickness ($\sqrt{D_e\overline{T_a}/R}$) over a time scale $\overline{T_a}$, the behavior is practically identical to that obtained with an infinite rock matrix thickness ($M, N \to 1$, Section S.2). For smaller values of B, matrix storage is limited, and matrix diffusion will not influence the power spectrum at lower frequencies. The mean total travel

time, given by $\overline{T}_a\left(1+2B\phi_m/b\right)$, is much longer than the mean advective travel time. It is independent of the matrix diffusion parameters but controlled by the total storage ratio $2B\phi_m/b$. For an infinite matrix, the total travel time is theoretically unbounded.

It is clear from Equation 15 that for strong matrix diffusion (large A; M, N close to 1), the third term in the denominator of Equation 15 dominates and the catchment spectral filter $S_{C_oC_o}/S_{C_iC_i}$ will exhibit 1/frequency behavior. More generally, Equation 15 can produce stream concentration power spectra with a range of apparent decay exponents >-2 (fractal scaling). When $A \to 0$ (negligible matrix diffusion) or $B \to 0$ (negligible matrix thickness), Equation 15 reduces to $S_{C_oC_o}(\omega) = S_{C_iC_i}(\omega)/\left(1+\omega^2\overline{T}_a^{\,2}\right)$, which corresponds to pure advection with an exponential advective travel time distribution across streamlines (Gelhar, 1993). It is also interesting to note that for a sorbing solute, Equation 15 predicts that in the frequency range where the third term in the denominator is dominant, the stream concentration power spectrum is $1/R$ times that for a passive solute. This is consistent with the behavior suggested by Feng et al. (2004).

Figure 2a shows the behavior of the spectral ratio or filter $S_{C_oC_o}/S_{C_iC_i}$ for different values of A (0, 2, 5, and 10) and $B/\sqrt{De\overline{T}_a}$ (5, 10, and ∞) for $A=5$, assuming no sorption $(R=1)$. For $A=5$ and 10, $1/\omega$ behavior is evident across several orders of magnitude in frequency. For $A=2$, behavior close to $1/\omega$ is evident at dimensionless frequencies between 0.1 and 10 (two orders of magnitude), with $1/\omega^{1.5}$ behavior at higher dimensionless frequencies. In general, the spectral ratio in Figure 2a exhibits curvature and deviates from true linear behavior in a log-log plot. However, the curvature is relatively mild at dimensionless frequencies >0.1. The scatter inherent in spectral estimates from noisy real-world data may obscure such curvature and accommodate acceptable straight-line fits. A finite matrix width does not influence the spectral ratio at high frequencies corresponding to time scales smaller than the diffusion time scale across the width. At lower frequencies, spectral ratios for a finite matrix width deviate from that for an infinite matrix and become steeper. This steepening could in fact produce a closer tendency to straight-line behavior when estimating spectra from noisy data (see $1/\omega$ line plotted in Figure 2a).

Strictly speaking, fractal stream chemistry requires $1/\omega$ behavior (more generally spectral slopes >-2) persisting out to very high frequencies (Kirchner et al., 2000). While the matrix diffusion model will produce $1/\omega^2$ behavior for $\omega\overline{T}_a > \sim 10A^2$, this dimensionless frequency value is quite large even for modest values of A. In a wide range of relevant frequencies, apparent spectral slopes produced by matrix diffusion will be closer to -1 or -1.5, and thus consistent with fractal scaling. Matrix diffusion produces frequency-dependent attenuation of the power spectrum generated purely by the advective travel time distribution, with maximum attenuation at $\omega\overline{T}_a \sim 1$. There is little attenuation at extremely low $(\omega\overline{T}_a < 1/\left(10A^2\right))$ frequencies because the spectral content of the input forcing at time scales much longer than the characteristic response time scales of any system is preserved. The lack of attenuation at high $(\omega\overline{T}_a > 10A^2)$ frequencies is because matrix diffusion does not influence very early time advective breakthrough (explained in Section 4). At intermediate-high frequencies, the frequency domain signature of fracture-matrix coupling ($\sqrt{i\omega}$, second term in $k(\omega)$) generates fractal scaling. The resulting attenuated spectral ratio resembles that of a gamma $(\alpha=0.5)$ total travel time distribution whose mean total travel time is much longer than the mean advective travel time $\overline{T}_a$. At lower frequencies, the spectral ratio influenced by matrix diffusion does not flatten out as much as that generated by the advective travel time distribution (due to the slow delayed release of solutes), sustaining fractal scaling with an apparent spectral slope between -1 and -0.5. From Equation 14, a generalization of Equation 15 for a gamma advective travel time distribution is presented in the SI (Section S.2, Equation S25). With a shape parameter α, the $1/\omega^{2\alpha}$ scaling in the spectral ratio of a gamma advective travel time distribution is modified to $1/\omega^{\alpha}$ by matrix diffusion for large A.

4. Time Domain Analysis: Solute Travel Time Distribution (TTD)

The solute TTD $h(t)$ is the solution for $C_o(t)$ corresponding to a unit impulse (Dirac delta) input, that is, $C_i(t)=\delta(t)$, and can be obtained from Equation 7. The solution for $C_f\left(T_a,t;I_{T_a}\right)$ at the outflow end of any streamline due to a unit impulse at the inflow, can be expressed in the form $H\left(t-T_a\right)g\left(T_a;t-T_a\right)$, where $H\left(t-T_a\right)$ is the Heaviside function. The function g depends on both the advective travel time T_a and the time

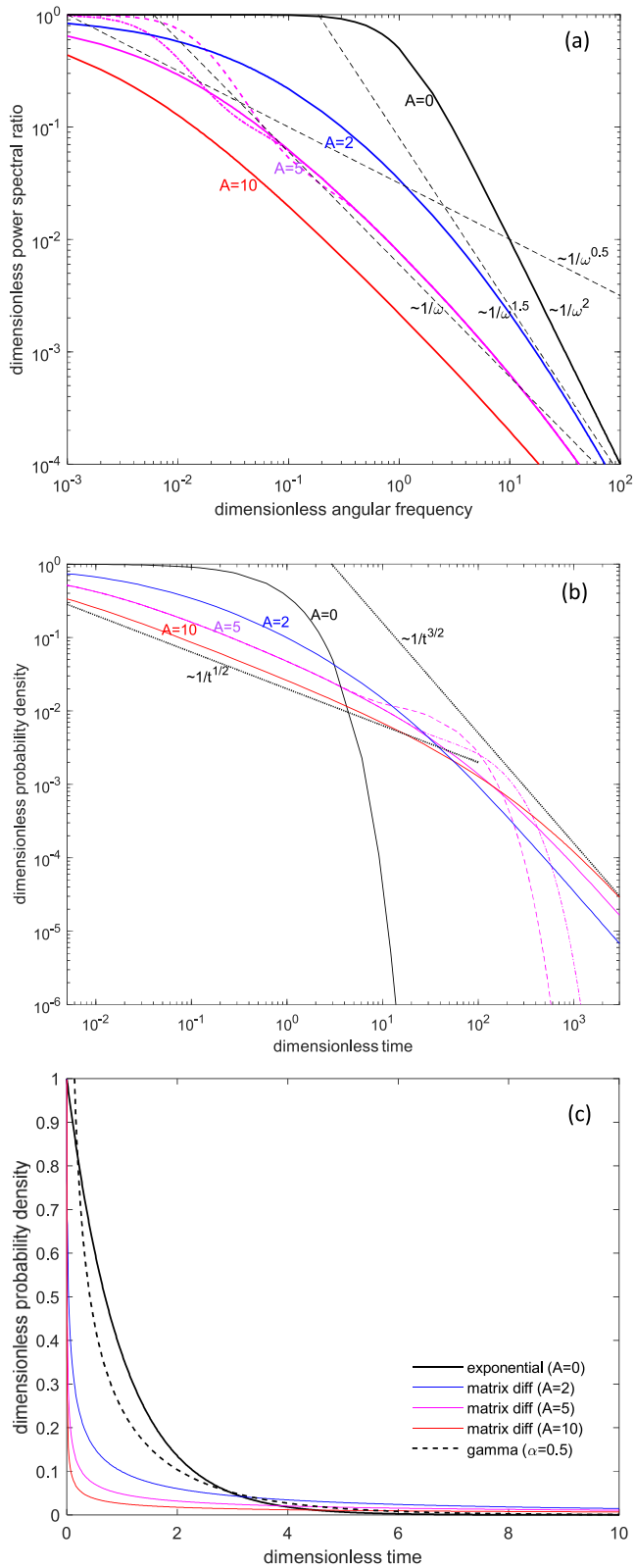
(a)
dimensionless power spectral ratio
dimensionless angular frequency
A=0
A=2
A=5
A=10
~1/ω^0.5
~1/ω
~1/ω^1.5
~1/ω^2
(b)
dimensionless probability density
dimensionless time
A=0
A=2
A=5
A=10
~1/t^3/2
~1/t^1/2
(c)
dimensionless probability density
dimensionless time
exponential (A=0)
matrix diff (A=2)
matrix diff (A=5)
matrix diff (A=10)
gamma (α=0.5)

Figure 2.

since advective breakthrough, $t - T_a$. It has a simple analytical form for an infinite matrix (Małoszewski & Zuber, 1985, Section S.4):

$$g\left(T_a;t-T_a\right)=\frac{aT_a}{\sqrt{\pi}\left(t-T_a\right)^{3/2}}\exp\left(-\frac{a^2T_a^2}{\left(t-T_a\right)}\right) \tag{17}$$

where $a=\phi_m\sqrt{RD_e}/b$. However, $g\left(T_a;t-T_a\right)$ can only be expressed as an implicit integral or obtained by numerical Laplace transform inversion for finite matrix widths (Małoszewski & Zuber, 1985, Section S.3). In either case, $h\left(t\right)$ can be expressed from Equation 7 as:

$$h\left(t\right)=\int_0^\infty H\left(t-T_a\right)g\left(T_a;t-T_a\right)P\left(T_a\right)dT_a=\int_0^t g\left(T_a;t-T_a\right)P\left(T_a\right)dT_a \tag{18}$$

At any time t after input, the solute TTD (Equation 18) only includes contributions from streamlines for which the advective travel time to the stream $T_a \le t$. It accounts for the combined influence of variable advective travel times across streamlines (with any appropriate form for $P\left(T_a\right)$) and matrix diffusion. Cvetkovic et al. (1999), Simic and Destouni (1999), Cvetkovic and Haggerty (2002), Lindgren et al. (2004), and Cvetkovic et al. (2012) employed similar approaches for advective travel time distributions generated by heterogeneity.

Figures 2b and 2c show the dimensionless solute TTD $h\left(t/\overline{T}_a\right)\overline{T}_a$ obtained by numerical integration of Equation 18 with the exponential $P\left(T_a\right)$ from Equation 8 in log-log and linear plots. The TTD for $A = 0$ (no matrix diffusion) is the exponential distribution. Analytical approximations to Equation 18 for infinite matrix widths are presented in Section S.4 (for both exponential and gamma $P\left(T_a\right)$). With an exponential $P\left(T_a\right)$, power-law behavior ($h\left(t\right) \sim t^{-1/2}$), similar to the gamma distribution with $\alpha = 0.5$, arises at intermediate times (Equation S35, Section S.4):

$$h\left(\frac{t}{\overline{T}_a}\right)\overline{T}_a \approx \frac{1}{2\sqrt{A\pi}}\left(\frac{t}{\overline{T}_a}\right)^{-1/2},\frac{1}{A}<\frac{t}{\overline{T}_a}<4A^2 \tag{19}$$

This behavior, evident in Figures 2b and 2c, is also valid for finite matrix widths, which only influence late time behavior. However, unlike a gamma distribution, the TTD does not blow up as $t \to 0$, instead approaching $P\left(t\right)$, the advective travel time distribution. For any value of A, at very early times $\left(t,T_a \to 0\right)$, it can be shown that $g\left(T_a;t-T_a\right) \to \delta\left(t-T_a\right)$ and thus $h\left(t\right) \to P\left(t\right)$ (also see Figures S1 and S2). Furthermore, the explicit dependence of g on T_a in addition to $t - T_a$ is such that streamlines with shorter T_a are less affected by matrix diffusion than streamlines with longer T_a. Thus, the overall TTD influenced by matrix diffusion exhibits a much steeper decline (steepness increasing with A) at intermediate times, compared to an exponential TTD. Solute retained by matrix diffusion is released slowly at later times, producing longer and heavier tails. For an infinite matrix, the late-time tail behaves as $h\left(t\right) \sim t^{-3/2}$ (Section S.4) and the mean total travel time is unbounded. For finite matrix widths (shown for $A = 5$), the solute TTD coincides with that for an infinite matrix at earlier times, then levels off due to back-diffusion of solute from the matrix, and subsequently decreases exponentially as solute is flushed out. The mean total travel time ($\overline{T}_a\left(1+2B\phi_m/b\right)$) is much longer than the mean advective travel time $\overline{T}_a$.

Overall, the solute TTD impacted by matrix diffusion thus exhibits both the steep decline (short-term responsiveness) similar to a gamma distribution with $\alpha = 0.5$, and long-term memory, which are highlighted by Kirchner et al. (2000) as key elements of fractal scaling. In Section S.4, I also consider gamma advective travel time distributions with shape parameter $0 < \alpha < 2$, showing that Equation 19 generalizes to $h\left(t\right) \sim t^{-1+\alpha/2}$, allowing for a wider range of intermediate-time power-law behaviors.

Figure 2. Influence of the matrix diffusion parameter A. (a) Dimensionless power spectral ratio $\left(S_{C_oC_o}/S_{C_iC_i}\right)$ Equation 15 plotted against dimensionless angular frequency ($\omega\overline{T}_a$). Black lines indicate various power-law slopes. For $A = 0$ (solid black), $S_{C_oC_o}/S_{C_iC_i}\left(\omega\right)=\left(1+\omega^2\overline{T}_a^2\right)$. (b and c) Dimensionless solute travel time distribution (TTD) $h\left(t/\overline{T}_a\right)\overline{T}_a$ from Equation 18 with an exponential $P\left(T_a\right)$, plotted against dimensionless time ($t/\overline{T}_a$) on logarithmic (b) and linear (c) axes. Solid lines correspond to different values of A and an infinite matrix. The dashed and dash-dotted magenta lines in (b) correspond to $B/\sqrt{D_e\overline{T}_a}=5$ and 10 respectively, for $A = 5$. Black dotted lines show intermediate ($\sim 1/t^{1/2}$) and late-time ($\sim 1/t^{3/2}$) power-law regimes. A dimensionless gamma TTD with shape parameter $\alpha = 0.5$ is shown in (c) for comparison.

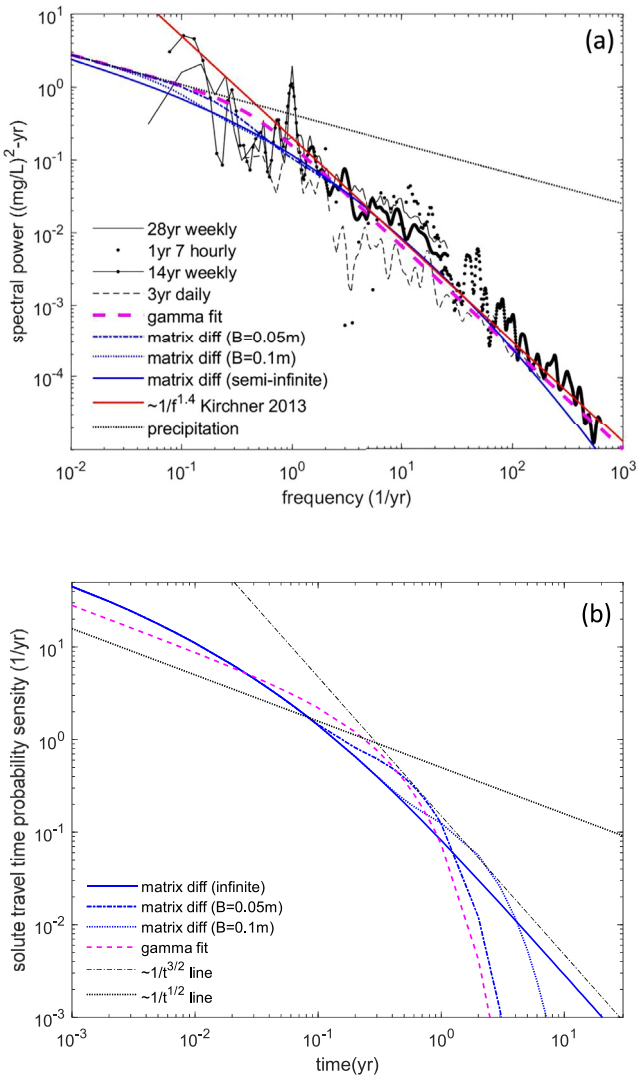

Figure 3. (a) Chloride power spectrum and (b) solute travel time distribution (TTD) for Lower Hafren, based on the matrix diffusion model ($\phi_m = 0.15, D_e = 1.5\times10^{-10}\,\mathrm{m}^2/\mathrm{s}, b = 5\times10^{-4}\,\mathrm{m}, \overline{T}_a = 0.01\mathrm{yr}$) and matrix widths $B = 0.05$ m, 0.1 m, and ∞; and a gamma model ($\alpha = 0.5, \beta = 0.4\mathrm{yr}$) fit to the power spectral estimates from Kirchner and Neal (2013). A line with the fitted power law slope of −1.4 (Kirchner & Neal, 2013) is also shown in (a). Dotted and dash-dotted lines in (b) respectively show the intermediate ($\sim 1/t^{1/2}$) and late-time ($\sim 1/t^{3/2}$) power-law regimes.

5. Application to the Lower Hafren Catchment

Neal et al. (1997) describe the hydrogeology of the Hafren catchment. Storm runoff is dominated by groundwater and interflow, and groundwater levels are highly responsive to rainfall. The shallow groundwater system is hosted in highly fractured shale, mudstone, and greywacke rocks, overlain by relatively thin soils (~0.7 m). Typical water table depths are around 5 m. Although groundwater is estimated to occur down to 30 m below the stream, rapid circulation and significant groundwater storage only occurs down to 9 m depth, suggesting a saturated thickness (H) of ~4 m for the active portion of the groundwater system. The net recharge rate (r) is about 2 m/year.

Kirchner et al. (2000) and Kirchner and Neal (2013) presented stream and precipitation power spectra for chloride at Lower Hafren. Both analyses suggest that the power spectral ratio $S_{C_oC_o}(\omega)/S_{C_iC_i}(\omega)$ exhibits close to $1/\omega$ behavior, well represented by a gamma solute TTD, for which $S_{C_oC_o}(f)/S_{C_iC_i}(f) = 1/(1+4\pi^2 f^2\beta^2)^{\alpha}$, where $f = \omega/2\pi$ is the frequency. Kirchner et al. (2000) fitted values of $\alpha = 0.48, \beta = 1.9\mathrm{yr}$, which corresponds to a mean total travel time of $\alpha\beta = 0.91\mathrm{yr}$. The power spectra of Kirchner and Neal (2013) are better fit with $\alpha = 0.5, \beta = 0.4\mathrm{yr}$ (Figure 3a), which corresponds to a shorter mean travel time of 0.2 years. Kirchner and Neal (2013) reported that the precipitation chloride spectrum exhibits $1/f^{0.41}$ behavior. From a precipitation chloride spectrum based on a subset of the full data set (Harman, 2015), I obtained a best fit of $0.38/f^{0.34}$ (mg/L)^2-yr. With the exponent fixed at 0.41, I obtained a best fit $0.42/f^{0.41}$ (mg/L)^2-yr. These two alternative forms for the precipitation chloride spectra do not produce major differences in calculated stream concentration spectra (compare Figure 3a with Figure S4).

The power spectral ratio (15, 16) depends on two key variables: the mean advective travel time $\overline{T}_a$ and the matrix diffusion parameter A. Because A contains products and ratios of other physical parameters, these parameters cannot be fit uniquely. My intention here is not to produce a "best-fit" parameter set, but rather to present reasonable parameter values that are consistent with the site description and match the spectral estimates of Kirchner and Neal (2013). I assume an exponential advective travel time distribution (Equation 8). Estimation of $\overline{T}_a$ requires an estimate of the effective fracture porosity ϕ_a for the hydrologically responsive flow system at the scale of the watershed, which is a highly uncertain parameter. Assuming a value of $\phi_a = 0.005$ (e.g., a regular arrangement of cubic matrix blocks with 0.3 m sides, interspersed with $b = 0.5$ mm wide connected fractures), the mean advective travel time is estimated as $\overline{T}_a = \phi_a H/r = 0.01$ years (3.65 days). The accessible matrix width B in Equations 15 and 16 could be smaller than the block size, first, Barker's (1985) analysis suggests an effective width equal to 1/6 of the block size for cubical blocks, and second, significant matrix diffusion is often restricted to the weathered periphery of matrix blocks. Assumed values for the matrix porosity ($\phi_m = 0.15$), and effective diffusivity for chloride ($D_e = 1.5\times10^{-10}$ m^2/s) fall within the ranges reported for shale and mudstone (Barone et al., 1992; Manger, 1963), resulting in $A = 2.06$.

Figure 3a compares $S_{C_oC_o}(f)$ calculated using $S_{C_iC_i}(f) = 0.42/f^{0.41}$ and the above parameter values in Equation 15, the gamma model with $\alpha = 0.5, \beta = 0.4\mathrm{yr}$, and the spectral estimates from Figure S7 in Kirchner and Neal (2013). Both the matrix diffusion and the fitted gamma models produce reasonable matches to the estimated stream concentration spectra and the slope of −1.4 estimated by Kirchner and Neal (2013). Because of the relatively short $\overline{T}_a$, even a small accessible matrix thickness ($B = 0.05m, B/\sqrt{D_e\overline{T}_a} = 7.27$) produces only a minor deviation of the power spectral ratio from that for an infinite matrix. All models

approach the precipitation concentration spectrum at frequencies <0.1 yr^{-1}. At the high frequency end (>20 yr^{-1}), the matrix diffusion models underestimate the spectral power slightly. This is likely because the analysis assumes steady flow and thus misses the influence of hydrologic transients. Alternative sets of parameter values that produce reasonable matches with the estimated stream concentration spectra are presented in Figure S3. As noted above, compensatory variations among the physical parameters that occur in A preclude unique parameter estimates.

The solute TTDs corresponding to the power spectral models presented in Figure 3a are shown in Figure 3b. For finite matrix widths ($B = 0.05$, 0.1 m), the solute TTDs obtained with the matrix diffusion model are comparable to the fitted gamma distribution, which exhibits $t^{-1/2}$ power law behavior at intermediate times. The tails of the solute TTDs are longer for larger B, and for very large B, there is a tendency toward $t^{-3/2}$ behavior at late time. The mean solute travel times corresponding to the finite width matrix diffusion models are 0.31 years ($B = 0.05$ m) and 0.61 years ($B = 0.1$ m).

6. Discussion

Although the role of matrix diffusion in influencing environmental solute ages has been recognized previously, it is seldom explicitly considered in studies and interpretations of catchment solute TTDs. This paper quantitatively demonstrates that matrix diffusion in fractured bedrock can generate fractal stream chemistry, power-law behavior and long-term memory in solute TTDs. The general relationships Equation 14 and Equation 18 provide a framework for quantifying catchment-scale stream concentration power spectra and solute TTDs, by superposing the influence of matrix diffusion on any general advective travel time distribution derived from analytical or numerical subsurface flow models (e.g., Ameli et al., 2016; Carroll et al., 2020; Kollet & Maxwell, 2008). The matrix diffusion mechanism is physically consistent with the large residual or passive storage component inferred while calibrating compartmental models of catchment hydrochemical response (e.g., Birkel et al., 2011; Benettin et al., 2015). The analysis presented here can also be extended to incorporate alternative representations of matrix diffusion and retention (e.g., multirate models or memory functions) and heterogeneity within the fracture flow system (Berkowitz et al., 2006; Cvetkovic & Haggerty, 2002; Shapiro, 2001; Zhou et al., 2007).

In a data-rich setting like the catchments at Plynlimon, availability of high frequency long-term datasets on precipitation and stream water chemistry and hydrogeologic characterization provides constraints on parameters in the matrix diffusion model. In general, application of the matrix diffusion model will require estimates of the matrix diffusion parameter $A = \phi_m \sqrt{R D_e \overline{T_a}}/b$, in which the porous medium and fracture properties appear as a product. It is therefore challenging to estimate these parameters uniquely. This nonuniqueness issue is unavoidable if only input-output water chemistry data are available. The influence of matrix diffusion would be confirmed if spectra for nonreactive solutes with different molecular diffusivities exhibit distinct differences (A would be expected to vary in the ratio of the square root of their molecular diffusivities). Rock matrix porosity ϕ_m and effective diffusivity D_e can be estimated from experimental measurements on rock samples. There is typically less heterogeneity in these properties, compared to permeability. It is more appropriate to estimate the average fracture aperture b from fitted TTDs, since it varies substantially and represents a catchment-scale parameter. Similar comments apply to constraining the mean advective travel time $\overline{T_a}$, which requires estimates of recharge, saturated thickness and active porosity in the Dupuit model. More generally, where the Dupuit model is not valid, the geometry of streamlines will be influenced by subsurface stratigraphy (including declining permeability with depth and distinct geological units), and better represented using numerical groundwater flow models. The influence of matrix diffusion can also be incorporated into numerical models of transient unsaturated-saturated flow and transport (e.g., Carroll et al., 2020; Kollet & Maxwell, 2008) for more comprehensive evaluation of solute TTDs. Interpretation of solute TTDs, especially in mountain catchments with fractured bedrock, should consider the potential influence of matrix diffusion in addition to other factors.

Data Availability Statement

No datasets were generated in this study.

Acknowledgments
This research was supported partially by National Science Foundation award EAR2012264. The author is grateful to James Kirchner for his comments and for providing the power spectral estimates from Lower Hafren, which are available in Figure S7 from Kirchner and Neal (2013). He also thanks Bhavna Arora and editor Valeriy Ivanov for their comments.

References

Ameli, A. A., Amvrosiadi, N., Grabs, T., Laudon, H., Creed, I. F., McDonnell, J. J., & Bishop, K. (2016). Hillslope permeability architecture controls on subsurface transit time distribution and flow paths. *Journal of Hydrology*, *543*, 17–30. https://doi.org/10.1016/j.jhydrol.2016.04.071

Barker, J. A. (1985). Block geometry functions characterizing transport in densely fissured media. *Journal of Hydrology*, *77*, 263–279. https://doi.org/10.1016/0022-1694(85)90211-2

Barone, F. S., Rowe, R. K., & Quigley, R. M. (1992). Estimation of chloride diffusion coefficient and tortuosity factor for mudstone. *ASCE Journal of Geotechnical Engineering*, *118*(7), 1992. https://doi.org/10.1061/(ASCE)0733-9410

Benettin, P., Kirchner, J. W., Rinaldo, A., & Botter, G. (2015). Modeling chloride transport using travel time distributions at Plynlimon, Wales. *Water Resources Research*, *51*, 3259–3276. https://doi.org/10.1002/2014WR016600

Berkowitz, B., Cortis, A., Dentz, M., & Scher, H. (2006). Modeling non-Fickian transport in geological formations as a continuous time random walk. *Reviews of Geophysics*, *44*, RG2003. https://doi.org/10.1029/2005rg000178

Birkel, C., Soulsby, C., & Tetzlaff, D. (2011). Modelling catchment-scale water storage dynamics: Reconciling dynamic storage with tracer inferred passive storage. *Hydrological Processes*, *25*(25), 3924–3936. https://doi.org/10.1002/hyp.8201

Botter, G., Bertuzzo, E., & Rinaldo, A. (2010). Transport in the hydrologic response: Travel time distributions, soil moisture dynamics, and the old water paradox. *Water Resources Research*, *46*, W03514. https://doi.org/10.1029/2009WR008371

Cardenas, M. B. (2007). Potential contribution of topography-driven regional groundwater flow to fractal stream chemistry: Residence time distribution analysis of Toth flow. *Geophysical Research Letters*, *34*, L05403. https://doi.org/10.1029/2006GL029126

Carroll, R. W. H., Deems, J. S., Niswonger, R., Schumer, R., & Williams, K. H. (2019). The importance of interflow to groundwater recharge in a snowmelt-dominated headwater basin. *Geophysical Research Letters*, *46*, 5899–5908. https://doi.org/10.1029/2019GL082447

Carroll, R. W. H., Manning, A. H., Niswonger, R., Marchetti, D., & Williams, K. H. (2020). Baseflow age distributions and depth of active groundwater flow in a snow-dominated mountain headwater basin. *Water Resources Research*, *56*, e2020WR028161. https://doi.org/10.1029/2020WR028161

Cvetkovic, V., Carstens, C., Selroos, J.-O., & Destouni, G. (2012). Water and solute transport along hydrological pathways. *Water Resources Research*, *48*, W06537. https://doi.org/10.1029/2011WR011367

Cvetkovic, V., & Haggerty, R. (2002). Transport with multiple-rate exchange in disordered media. *Physical Review E - Statistical Physics, Plasmas, Fluids, and Related Interdisciplinary Topics*, *65*, 051308. https://doi.org/10.1103/PhysRevE.65.051308

Cvetkovic, V., Selroos, J., & Cheng, H. (1999). Transport of reactive tracers in rock fractures. *Journal of Fluid Mechanics*, *378*, 335–356. https://doi.org/10.1017/S0022112098003450

Duffy, C. J., & Gelhar, L. W. (1985). A frequency domain approach to water quality modeling in groundwater: Theory. *Water Resources Research*, *21*(8), 1175–1184. https://doi.org/10.1029/WR021i008p01175

Duffy, C. J., & Gelhar, L. W. (1986). A frequency domain analysis of groundwater quality fluctuations: Interpretation of field data. *Water Resources Research*, *22*(7), 1115–1128. https://doi.org/10.1029/WR022i007p01115

Feng, X., Kirchner, J. W., & Neal, C. (2004). Measuring catchment-scale chemical retardation using spectral analysis of reactive and passive chemical tracer time series. *Journal of Hydrology*, *292*, 296–307. https://doi.org/10.1016/j.jhydrol.2004.01.012

Fiori, A., & Russo, D. (2008). Travel time distribution in a hillslope: Insight from numerical simulations. *Water Resources Research*, *44*, W12426. https://doi.org/10.1029/2008WR007135

Foster, S. S. D. (1975). The Chalk groundwater tritium anomaly: A possible explanation. *Journal of Hydrology*, *25*(1–2), 159–165. https://doi.org/10.1016/0022-1694(75)90045-1

Frisbee, M. D., Wilson, J. L., Gomez-Velez, J. D., Phillips, F. M., & Campbell, A. R. (2013). Are we missing the tail (and the tale) of residence time distributions in watersheds? *Geophysical Research Letters*, *40*, 4633–4637. https://doi.org/10.1002/grl.50895

Gelhar, L. W., (1993). *Stochastic subsurface hydrology* (p. 390). Prentice-Hall.

Gelhar, L. W., & Collins, M. A. (1971). General analysis of longitudinal dispersion in nonuniform flow. *Water Resources Research*, *7*(6), 1511–1521. https://doi.org/10.1029/WR007i006p01511

Gelhar, L. W., & Wilson, J. L. (1974). Ground-water quality modeling. *Ground Water*, *12*, 399–408. https://doi.org/10.1111/j.1745-6584.1974.tb03050.x

Godsey, S. E., Aas, W., Clair, T. A., de Wit, H. A., Fernandez, I. J., Kahl, J. S., et al. (2010). Generality of fractal 1/f scaling in catchment tracer time series, and its implications for catchment travel time distributions. *Hydrological Processes*, *24*, 1660–1671. https://doi.org/10.1002/hyp.7677

Haitjema, H. M. (1995). On the residence time distribution in idealized groundwatersheds. *Journal of Hydrology*, *172*(1– 4), 127–146. https://doi.org/10.1016/0022-1694(95)02732-5

Hale, V. C., McDonnell, J. J., Stewart, M. K., Solomon, D. K., Doolitte, J., Ice, G. G., & Pack, R. T. (2016). Effect of bedrock permeability on stream base flow mean transit time scaling relationships: 2. Process study of storage and release. *Water Resources Research*, *52*, 1375–1397. https://doi.org/10.1002/2015WR017660

Harman, C. J. (2015). Time-variable transit time distributions and transport: Theory and application to storage-dependent transport of chloride in a watershed. *Water Resources Research*, *51*, 1–30. https://doi.org/10.1002/2014WR015707

Herndon, E. M., Dere, A. L. D., Sullivan, P. L., Norris, D., Reynolds, B., & Brantley, S. L. (2015). Landscape heterogeneity drives contrasting concentration–discharge relationships in shale headwater catchments. *Hydrology and Earth System Sciences Discussions*, *19*, 3333–3347. https://doi.org/10.5194/hess-19-3333-2015

Hrachowitz, M., Benettin, P., van Breukelen, B. M., Fovet, O., Howden, N. J., Ruiz, L., et al. (2016). Transit times: The link between hydrology and water quality at the catchment scale. *WIREs Water*, *3*, 629–657. https://doi.org/10.1002/wat2.1155

Hrachowitz, M., Savenije, H., Bogaard, T. A., Tetzlaff, D., & Soulsby, C. (2013). What can flux tracking teach us about water age distribution patterns and their temporal dynamics? *Hydrology and Earth System Sciences*, *17*(2), 533–564. https://doi.org/10.5194/hess-17-533-2013

Kirchner, J. W., Feng, X. H., & Neal, C. (2000). Fractal stream chemistry and its implications for contaminant transport in catchments. *Nature*, *403*(6769), 524–527. https://doi.org/10.1038/35000537

Kirchner, J. W., Feng, X. H., & Neal, C. (2001). Catchment-scale advection and dispersion as a mechanism for fractal scaling in stream tracer concentrations. *Journal of Hydrology*, *254*(1-4), 82–101. https://doi.org/10.1016/S0022-1694(01)00487-5

Kirchner, J. W., & Neal, C. (2013). Universal fractal scaling in stream chemistry and its implications for solute transport and water quality trend detection. *Proceedings of the National Academy of Sciences of the United States of America*, *110*(30), 12213–12218. https://doi.org/10.1073/pnas.1304328110

Kollet, S. J., & Maxwell, R. M. (2008). Demonstrating fractal scaling of baseflow residence time distributions using a fully-coupled groundwater and land surface model. *Geophysical Research Letters*, *35*, L07402. https://doi.org/10.1029/2008GL033215

Lindgren, G. A., Destouni, G., & Miller, A. V. (2004). Solute transport through the integrated groundwater-stream system of a catchment. *Water Resources Research*, *40*, W03511. https://doi.org/10.1029/2003WR002765

Małoszewski, P., & Zuber, A. (1982). Determining the turnover time of groundwater systems with the aid of environmental tracers: 1. Models and their applicability. *Journal of Hydrology*, *57*(3–4), 207–231. https://doi.org/10.1016/0022-1694(82)90147-0

Małoszewski, P., & Zuber, A. (1985). On the theory of tracer experiments in fissured rocks with a porous matrix. *Journal of Hydrology*, *79*(3–4), 333–358. https://doi.org/10.1016/0022-1694(85)90064-2

Maloszewski, P., & Zuber, A. (1993). Principles and practice of calibration and validation of mathematical models for the interpretation of environmental tracer data. *Advances in Water Resources*, *16*, 173–190. https://doi.org/10.1016/0309-1708(93)90036-F

Manger, G. E. (1963). *Porosity and bulk density of sedimentary rocks*. In Geological Survey Bulletin 1144-E. United States Geological Survey. Retrieved from https://pubs.usgs.gov/bul/1144e/report.pdf

Manning, A. H., Verplanck, P. L., Caine, J. S., & Todd, A. S. (2013). Links between climate change, water-table depth, and water chemistry in a mineralized mountain watershed. *Applied Geochemistry*, *37*, 64–78. https://doi.org/10.1016/j.apgeochem.2013.07.002

McGuire, K. J., & McDonnell, J. J. (2006). A review and evaluation of catchment transit time modeling. *Journal of Hydrology*, *330*(3–4), 543–563. https://doi.org/10.1016/j.jhydrol.2006.04.020

McGuire, K. J., McDonnell, J. J., Weiler, M., Kendall, C., McGlynn, B. L., Welker, J. M., & Seibert, J. (2005). The role of topography on catchment-scale water residence time. *Water Resources Research*, *41*, W05002. https://doi.org/10.1029/2004WR003657

Neal, C., Robson, A. J., Shand, P., Edmunds, W. M., Dixon, A. J., Buckley, D. K., et. al. (1997). The occurrence of groundwater in the Lower Palaeozoic rocks of upland Central Wales. *Hydrology and Earth System Sciences Discussions*, *1*, 3–18. https://doi.org/10.5194/hess-1-3-1997

Neretnieks, I. (1981). Age dating of groundwater in fissured rock: Influence of water volume in micropores. *Water Resources Research*, *17*(2), 421–422. https://doi.org/10.1029/WR017i002p00421

Shapiro, A. M. (2001). Effective matrix diffusion in kilometer-scale transport in fractured crystalline rock. *Water Resources Research*, *37*(3), 507–522. https://doi.org/10.1029/2000WR900301

Shapiro, A. M. (2011). The challenge of interpreting environmental tracer concentrations in fractured rock and carbonate aquifers. *Hydrogeology Journal*, *19*, 9–12. https://doi.org/10.1007/s10040-010-0678-x

Simic, E., & Destouni, G. (1999). Water and solute residence times in a catchment: Stochastic-mechanistic model interpretation of 18O transport. *Water Resources Research*, *35*(7), 2109–2119. https://doi.org/10.1029/1999WR900054

Sprenger, M., Stumpp, C., Weiler, M., Aeschbach, W., Allen, S. T., Benettin, P., et al. (2019). The demographics of water: A review of water ages in the critical zone. *Reviews of Geophysics*, *57*, 800–834. https://doi.org/10.1029/2018RG000633

Tang, D., Frind, E., & Sudicky, E. A. (1981). Contaminant transport in fractured porous media: Analytical solution for a single fracture. *Water Resources Research*, *17*(3), 555–564. https://doi.org/10.1029/WR017i003p00555

Tokunaga, T. K., Wan, J., Williams, K. H., Brown, W., Henderson, A., Kim, Y., et al. (2019). Depth- and time-resolved distributions of snowmelt-driven hillslope subsurface flow and transport and their contributions to surface waters. *Water Resources Research*, *55*. https://doi.org/10.1029/2019WR025093

Zhou, Q., Liu, H.-H., Molz, F. J., Zhang, Y., & Bodvarsson, G. S. (2007). Field-scale effective matrix diffusion coefficient for fractured rock: Results from literature survey. *Journal of Contaminant Hydrology*, *93*(1–4), 161–187. https://doi.org/10.1016/j.jconhyd.2007.02.002

References From the Supporting Information

Grisak, G., & Pickens, J.-F. (1980). Solute transport through fractured media: 1. The effect of matrix diffusion. *Water Resources Research*, *16*(4), 719–730. https://doi.org/10.1029/WR016i004p00719

Hyman, J. D., Rajaram, H., Srinivasan, S., Makedonska, N., Karra, S., Viswanathan, H., & Srinivasan, G. (2019). Matrix diffusion in fractured media: New insights into power law scaling of breakthrough curves. *Geophysical Research Letters*, *46*, 13785–13795. https://doi.org/10.1029/2019GL085454

McClure, T. (2020). *Numerical inverse Laplace transform*. In MATLAB Central File Exchange. Retrieved from https://www.mathworks.com/matlabcentral/fileexchange/39035-numerical-inverse-laplace-transform

Weisstein, E. W. (2021). Confluent hypergeometric function of the second kind. In *From MathWorld-A Wolfram web resource*. Retrieved from https://mathworld.wolfram.com/ConfluentHypergeometricFunctionoftheSecondKind.html